Unified slip boundary condition for fluid flows

Joseph John Thalakkottor and Kamran Mohseni

Phys. Rev. E **94**, 023113 — Published 26 August 2016

DOI: 10.1103/PhysRevE.94.023113

Unified slip boundary condition for fluid flows

Joseph John Thalakkottor[1,*] and Kamran Mohseni[1,2,†]

[1] *Department of Mechanical and Aerospace Engineering, University of Florida, Gainesville, FL.*

[2] *Department of Electrical and Computer Engineering, University of Florida, Gainesville, FL.*

(Dated: July 5, 2016)

Abstract

Determining the correct matching boundary condition is fundamental to our understanding of several everyday problems. Despite over a century of scientific work, existing velocity boundary conditions are unable to consistently explain and capture the complete physics associated with certain common but complex problems such as moving contact lines and corner flows. The widely used Maxwell and Navier slip boundary conditions make an implicit assumption that velocity varies only in the wall normal direction. This makes their boundary condition inapplicable in the vicinity of contact lines and corner points where, velocity gradient exists both in the wall normal and wall tangential directions. In this paper, by identifying this implicit assumption we are able to extend Maxwell's slip model. Here, we present a generalized velocity boundary condition that shows that slip velocity is a function of not only the shear rate but also the linear strain rate. In addition, we present a universal relation for slip length which shows that, for a general flow, slip length is a function of the principal strain rate. The universal relation for slip length along with the generalized velocity boundary condition provides a unified slip boundary condition to model a wide range of steady Newtonian fluid flows. We validate the unified slip boundary for simple Newtonian liquids, by using molecular dynamics simulations and studying both, the moving contact line and corner flow problems.

PACS numbers: 47.61.-k,83.50.Rp,68.08.-p,47.11.Mn

* tjjoseph@ufl.edu

† mohseni@ufl.edu

I. INTRODUCTION

The interface between two phases of matter is often accompanied by rapid changes in scales, multi-physics, geometrical complexities and intriguing chemical phenomena, making it an ideal benchmark to expand our knowledge beyond the confines of the bulk material. Determining the correct matching boundary conditions is essential for accurate predictions, as they govern the transfer of mass, momentum and energy across such interfaces. Among these, the boundary condition governing the transfer of tangential momentum across a fluid-solid interface is a topic that is still being debated, despite over a century of scientific work [1–7]. The no-slip boundary condition is known to be valid for many continuum scale problems. However, in some cases, such as spreading of fluid on a solid surface (moving contact line) [8–14], corner flow [15–17] and extrusion of polymer melts [18–20], assuming no-slip at the boundary leads to velocity and stress singularities, and the breakdown of the no-slip boundary condition. While steady flow boundary conditions for simple regular interfaces are fairly well understood [21–23], there is still a significant void in our understanding of the behavior near the intersection of multiple interfaces, such as a moving contact line (MCL) or a corner point. Here, the limiting factor is that the breakdown of the no-slip boundary condition at these intersections occurs at molecular scales. One of the proposed methods to alleviate these singularities is to assume fluid slip at these intersections. The two most common slip models are those presented more than a century ago, by Navier [24] and Maxwell [25]. However, Navier's and Maxwell's assumption of constant slip length for a given wall-fluid interface contradicts the findings presented in literature [10, 11], which shows perfect slip at the singular point and no-slip far away from it. Thompson & Troian [22] showed that at high shear rates slip length is no longer a constant but rather a function of the shear rate. They suggested that their model resolves this, as it naturally allows for varying degrees of slip on approaching regions of high shear stress and shear rate. However, as shall be shown in this paper, the non-linear relationship of slip with shear rate and the universality of their boundary condition is valid only for flows with velocity variation in the wall normal direction. Hence, the existing models [14, 22, 24, 25] are unable to consistently explain and capture the complete physics associated with more complex problems.

In this paper, we present a unified slip boundary condition that is applicable for a wide range of Newtonian fluid flow problems and includes the no-slip, Navier/Maxwell [24, 25],

and Thompson & Troian [22] velocity boundary conditions as limiting cases. The unified slip boundary condition, which is validated with molecular dynamics (MD) simulations, consists of two parts: First is the generalized velocity boundary condition, which accounts for the variation of flow velocity not only in the wall normal direction, as is the case for the Navier/Maxwell [24, 25] models, but also in the wall tangent direction. From this follows the second part where slip length is shown to be not just a constant, as suggested by Navier/Maxwell [24, 25], nor a non-linear function of just the shear rate, as suggested by Thompson & Troian [22], but rather a non-linear function of the principal strain rate. This universal relation for slip length along with the general velocity boundary condition provides a unified slip boundary condition to model a wide range of Newtonian fluid flows over a solid surface.

II. NUMERICAL SETUP

The molecular dynamics simulations presented in this paper are performed using the LAMMPS package [26]. The pairwise interaction of molecules, separated by a distance r, is modeled by the Lennard Jones (LJ) potential

$$V^{LJ} = 4\epsilon \left[\left(\frac{\sigma}{r}\right)^{12} - \left(\frac{\sigma}{r}\right)^{6} \right]. \tag{1}$$

Here, ϵ and σ are the characteristic energy and length scales, respectively. The potential is zero for $r > r_c = 2.5\sigma$, where r_c is the cutoff radius.

Each wall is comprised of at least two layers of molecules oriented along the (111) plane of a face centered cubic (fcc) lattice, with the molecules fixed to their respective lattice sites. The fluid molecules are initialized on a fcc lattice, with initial velocities randomly assigned so as to obtain the required temperature. The fluid in its equilibrium state, has a temperature $T = 1.1k_B/\epsilon$ and number density $\rho \approx 0.81\sigma^{-3}$ for the corner flow problem, and $\rho \approx 0.73\sigma^{-3}$ for the moving contact line problem. The temperature is maintained using a Langevin thermostat with a damping coefficient of $\Gamma = 0.1\tau^{-1}$, where $\tau = \sqrt{m\sigma^2/\epsilon}$ is the characteristic time and m is the mass of the fluid molecule. The damping term is only applied to the z direction to avoid biasing the flow. Table I, lists the different interfacial properties used in our study.

In this paper we consider both the moving contact line and the corner flow problems. In

TABLE I. **Parameters for different cases of wall-fluid interfacial properties with slip increasing from Case 1 to 4.** ϵ^{wf} and σ^{wf} are the Lennard-Jones (LJ) parameters for wall-fluid interaction and, ρ^w/ρ is relative density of wall. ϵ^{wf} determines the extent of affinity of the wall molecules to the fluid molecules and is inversely related to slip length. σ^{wf} corresponds to the molecular diameter or length scale associated with the LJ potential. An increase in its value leads to greater slip and vice-versa. Higher relative wall density (ρ^w/ρ) means a smoother perceived surface leading to greater slip.

Case	ϵ^{wf}/ϵ	σ^{wf}/σ	ρ^w/ρ
1	1.0	1.0	1.1
2	0.6	1.0	1.1
3	0.6	0.75	4.5
4	0.4	0.75	4.5

addition, we also simulate a single phase Couette flow to verify Thompson & Troian's [22] boundary condition.

Moving contact line: The moving contact line is simulated by modeling a two-phase, two dimensional Couette flow, where the fluid channel measures $153.0\sigma \times 27.4\sigma \times 144.0\sigma$. The walls move in opposite directions with a speed $U = 0.1\sigma/\tau$ and periodic boundary conditions are imposed along the x and z directions (Fig. 1(a)).

Corner flow: The corner flow is simulated by modeling a cavity flow with an inclined wall. The cavity measures $91.0\sigma \times 24.4\sigma \times 72.0\sigma$. The top and bottom walls move in opposite directions with a speed $U = 0.1\sigma/\tau$, while the side walls are stationary (Fig. 1(b)). A periodic boundary condition is imposed along the z direction, which is the out of plane axis. θ, describes the corner angle.

Single phase Couette flow: For the single phase Couette flow, the fluid channel measures $22.8\sigma \times 25.0\sigma \times 13.7\sigma$. The top wall moves with a speed $U = 0.1\sigma/\tau$, while the bottom wall is stationary. Periodic boundary conditions are imposed along the x and z directions.

In the case of the moving contact line problem the immiscibility of the two fluids is modeled by choosing appropriate LJ interaction parameters, such that the interatomic forces between them is predominantly repulsive. For the results presented here these parameters are $\epsilon^{f_1 f_2} = 0.2\epsilon$, $\sigma^{f_1 f_2} = 3.0\sigma$ and $r_c = 2.5\sigma$, which ensure a purely repulsive force. For simplicity the two fluids are assigned identical fluid properties.

The equations of motion are numerically integrated using the Verlet [27] algorithm with a time step $\Delta t = 0.002\tau$. The simulation is initially run until the flow equilibrates, after which spatial averaging is performed by dividing the fluid domain into rectangular bins of size $\sim 0.5 \times 1.0\sigma$ along the x–y plane, and extending through the entire depth of the channel. In addition to spatial averaging, time averaging is done for a duration of 8000τ for the moving contact line problem. In the case of a non-wetting wall, averaging was done for an extended time of 16000τ in order to resolve the data. For the corner flow problem time averaging is performed for a duration of 200000τ.

The velocity results presented in this paper are normalized by the wall velocity, $|U| = 0.1\sigma\tau^{-1}$. The dynamic viscosity of the bulk fluid is, $\mu = 1.9 \pm 0.2\epsilon\tau\sigma^{-3}$ and the Reynolds number of the flows is, $Re = 0.9 \pm 0.1$. In order to compute various quantities at the wall, a reference plane is defined at a distance of $1\sigma^{wf}$ away from the wall lattice site. For the single phase Couette flow problem, the velocity at the reference plane is evaluated by fitting the MD data with the analytical solution for a Couette flow. However, as there is no analytical solution for the MCL and the corner flow problem, the velocity at the reference plane is evaluated by linear extrapolation of the velocity to the reference plane. The strain rates are evaluated by discretizing the velocity field using a second order accurate finite difference scheme. Spurious data points at $2\sigma - 3\sigma$ away from the contact point and corner point are excluded as the data is unresolved.

Studies by Priezjev [28] and Pahlavan & Freund [29] have shown that the stiffness of thermal walls effect the slip length and its dependence on shear rate. It is also well known that the property of the secondary fluid in a two-phase flow governs the contact angle which in turn could effect the local stresses in the vicinity of the contact line in the primary fluid. In this paper, for simplicity and in order to isolate these effects, the test cases are modeled with wall molecules fixed to the lattice site and the two immiscible fluids having identical properties.

III. VERIFYING THOMPSON & TROIAN'S SLIP MODEL FOR A MOVING CONTACT LINE PROBLEM

Thompson and Troian showed that for high shear rates slip is no longer a constant rather it is a function of the shear rate. Their model provided a mechanism to relieve the stress singularity at contact lines and corner points. By scaling slip length (L_s) with its asymptotic value (L_s^o) and shear rate ($\dot{\gamma}$) with its critical value ($\dot{\gamma}_c$), they showed that the data for a steady Couette flow experiment collapses to a single universal curve, given by $L_s/L_s^o = (1 - \dot{\gamma}/\dot{\gamma}_c)^{-1/2}$. The reproduced results can be seen in, Fig. 2(a). However, the non-linear relationship of slip length with shear rate and the universality of their boundary condition were only demonstrated for a steady single phase flow. In order to verify their boundary condition for more complex flows, we perform MD simulations of a two-phase Couette flow (moving contact line problem). Using the values of L_s^o and $\dot{\gamma}_c$ obtained from the single phase Couette flow experiment, we scale the slip length and shear rate for the two-phase Couette flow. It is seen that Thompson & Troian's scaling does not result in collapsed data for the moving contact line problem (Fig. 2(b)). In addition, it is observed that the slip length starts to diverge even though the local shear rate has not approached the critical value. Similar results can be shown in the case of a corner flow.

IV. THE GENERALIZED VELOCITY BOUNDARY CONDITION

In order to address the limitations of existing models, Maxwell's slip model for rarefied gases [25] is revisited with the aim to identify the functionality associated with slip in a general steady fluid flow. Even though Maxwell's model [25, 30, 31] was established for rarefied gases, it is illustrated here that an analogous formulation shows promise to identify model functionalities for slip modeling in liquids, or fluids in general. This is emphasized by the fact that the Navier slip model gives the same functionality of slip velocity with shear rate as Maxwell. Similar steps were taken by Thalakkottor & Mohseni [32] to extend Maxwell's slip model to unsteady flows with success.

Maxwell proposed that the fluid molecules reflected by the wall can be divided into two categories namely, diffusive and specular reflection.

Diffusive reflection $\left(\boldsymbol{u}^{\text{diff}}\right)$: The incident fluid molecules can be imagined as being adsorbed by the wall and then emitted into the fluid, such that the net velocity will be the same as that of the fluid being at rest with respect to the wall, that is

$$u^{\text{diff}}(t_c^+) = \boldsymbol{s} \cdot \boldsymbol{U}(t_c). \tag{2}$$

Here, t_c is the time of collision, t_c^+ is the instantaneous time immediately after collision with the wall, $\boldsymbol{U}$ is the wall velocity vector and $\boldsymbol{s}$ is the wall-tangent unit vector. All the parameters are evaluated at the wall unless specified.

Specular reflection ($\boldsymbol{u}^{\text{spec}}$): The incident fluid molecules undergo perfect elastic collision with the wall, such that there is no tangential momentum transfer with the wall. Therefore,

$$u^{\text{spec}}(t_c^+) = \boldsymbol{s} \cdot \boldsymbol{u}(t_c^-), \tag{3}$$

where t_c^- is the instantaneous time immediately before collision and $\boldsymbol{u}$ is the fluid velocity adjacent to the wall. The velocity of the incident molecule is obtained by collision with a fluid molecule located at a distance away from the wall. Using the mean free path method [31, 33], the incident velocity can be calculated by performing a spatial discretization of the fluid velocity about the wall. Here, Maxwell and other researchers make an implicit assumption that the fluid velocity can only vary in the wall normal direction. Based on this assumption, they evaluate the Taylor series expansion of the fluid velocity, by computing the gradient of velocity only along the wall normal direction. However, for a general flow the fluid velocity is not limited to variation in only the wall normal direction and can also vary in the wall tangent direction. Therefore, using the mean free path method in three dimensions, we obtain

$$\begin{aligned} u^{\text{spec}}(t_c^+) &= \boldsymbol{s} \cdot \left(\boldsymbol{u}\left(t_c\right) - \boldsymbol{\Delta x} \cdot \boldsymbol{\nabla u}\left(t_c\right)\right) \\ &= \boldsymbol{s} \cdot \left(\boldsymbol{u}\left(t_c\right) - \frac{2}{3}\lambda \boldsymbol{\delta} \cdot \boldsymbol{\nabla u}\left(t_c\right)\right). \end{aligned} \tag{4}$$

$\boldsymbol{\Delta x}$ can be written as $\boldsymbol{\Delta x} = 2\lambda/3\boldsymbol{\delta}$, where $2\lambda/3$ is the average distance traveled by a molecule in the x, y and z directions in a mean free time, λ is the mean free path and $\boldsymbol{\delta} = (\pm 1, \pm 1, \pm 1)$ is the direction vector of the incident fluid molecule [31]. Hence, the spatial discretization of the fluid velocity, is the source of the primary difference between

the Maxwell slip model and our general velocity slip model and as will be seen, has significant ramifications on correct prediction near an interface irregularity.

Now, the momentum of diffusively reflected molecules together with specularly reflected molecules give the net momentum of the reflected molecules. The fractions of diffusive and specular molecules making up the net reflected molecules are determined by the tangential momentum accommodation coefficient ($\tilde{\sigma}$). Therefore, the net reflected velocity is written as

$$u(t_c^+) = \tilde{\sigma} u^{\text{diff}}(t_c^+) + (1 - \tilde{\sigma})\, u^{\text{spec}}(t_c^+). \tag{5}$$

As the incident and reflected velocities together constitute the actual fluid molecules close to the surface, the average fluid velocity at the wall is given as the mean of the velocity before and after collision,

$$u(t_c) = \frac{u(t_c^+) + u(t_c^-)}{2}. \tag{6}$$

By substituting and simplifying, the slip velocity can be written as

$$U_s = \frac{2}{3}\frac{(2 - \tilde{\sigma})}{\tilde{\sigma}} \lambda \boldsymbol{\delta} \cdot \nabla \boldsymbol{u} \cdot \boldsymbol{s}, \tag{7}$$

where $U_s = \boldsymbol{s} \cdot \boldsymbol{U} - \boldsymbol{s} \cdot \boldsymbol{u}$. The velocity gradient tensor can further be written as the sum of a symmetric (strain rate) and anti-symmetric (rotation rate) tensor, $\nabla \boldsymbol{u} = 1/2(\nabla \boldsymbol{u} + \nabla \boldsymbol{u}^T) + 1/2(\nabla \boldsymbol{u} - \nabla \boldsymbol{u}^T)$. It is known [14] and we have independently verified that slip velocity is independent of the rotation rate tensor. This is because the rotation rate tensor does not cause any strain in the fluid element. Therefore, the generalized velocity boundary condition is given by

$$U_s = L_s \boldsymbol{\delta} \cdot \frac{1}{2}(\nabla \boldsymbol{u} + \nabla \boldsymbol{u}^T) \cdot \boldsymbol{s}. \tag{8}$$

Here, the coefficient $[2\,(2 - \tilde{\sigma})\,\lambda]/3\tilde{\sigma}$ is a measure of slip at the interface and is replaced by slip length, L_s. This allows the model to be applicable for liquids as well, for which the mean free path is not well defined.

If we consider a two dimensional problem, then the above slip model simplifies to $U_s = L_s \left[\frac{\partial u}{\partial s} + \frac{\partial u}{\partial n}\right]$, where $\boldsymbol{n}$ is the wall-normal unit vector. Comparing to the Navier/Maxwell [24, 25] slip model, it is seen that the slip velocity has an additional dependency on the linear strain rate, $\partial u/\partial s$. It is known that far away from the corner or contact line $\partial u/\partial s$ reduces to zero, yielding the Navier/Maxwell boundary condition. Thus, their models can be viewed as a limiting case of the more general velocity boundary condition presented here.

Qian et. al [34] derived their Generalized Navier boundary condition based on a force balance argument, which says that slip is proportional to the tangential fluid force, $\beta U_s = \int_0^{z_0} dz(\partial_x \tilde{\sigma}_{xx} + \partial_z \tilde{\sigma}_{zx})$. Here, β is the slip coefficient, z_0 is the boundary layer thickness and $\tilde{(.)}$ refers to the hydrodynamic part of the stress. It can be seen that even though our respective approach in deriving the boundary condition are different, they too account for the linear stress similar to the linear strain rate in our boundary condition. This further justifies our generalized velocity boundary condition. However, in order to use the slip boundary condition, slip length needs to be known a priori. This is addressed next.

V. UNIVERSAL CURVE

The above findings suggest that for an arbitrary flow, slip length must not just be a function of shear rate [22], but rather a function of a flow parameter that captures the total strain rate experienced in a fluid element. One such parameter is the principal strain rate, which represents the maximum and minimum strain rate in a fluid element. It must be noted that for simple flows where velocity varies in only the wall normal direction, the principal strain rate is equivalent to the shear rate. Thus principal strain rate can be considered as the more general parameter. This is validated using MD simulations, for a moving contact line and a corner flow. The schematics of the problem are shown in Fig. 1 and the different wall-fluid properties used are listed in Table I.

The variation of slip length versus the local principal strain rate for a moving contact line problem is plotted in Fig. 3 and 4, for the trailing and leading edge, respectively. The principal strain rate for a 2D case is evaluated as $e_{1,2} = (e_{xx} + e_{yy})/2 \pm \sqrt{((e_{xx} - e_{yy})/2)^2 + e_{xy}^2)}$, where $e_{xx} = \partial u/\partial x$, $e_{yy} = \partial v/\partial y$ and $e_{xy} = 1/2(\partial u/\partial y + \partial v/\partial x)$. Depending on whether we are considering the leading or trailing edge, the principal strain rate e_1 or e_2 are used, respectively. e_1 represents the maximum extension experienced by the fluid which corresponds to the acceleration of the fluid as it moves away from the leading edge, while e_2 corresponds to the maximum compression corresponding to the deceleration of the fluid on approaching the trailing edge. In addition we also present the results for a corner flow with the wall moving towards and away from the corner, as shown in Fig. 5 and 6, respectively. We observe a non-linear relationship between slip length and principal strain rate, the functional behavior of which suggests the existence of a universal curve. Scaling slip length by its asymptotic

value and the principal strain rate ($e_{1,2}$) by its critical value (e_c), the data collapses onto a single curve, described by $L_s = L_s^o(1 - e_{1,2}/e_c)^\alpha$. The MD results show that α is approximately -0.5, Fig. 7. This relation implies that close to the critical principal strain rate, slip lengths would approach macroscopic values and at the critical value one would observe perfect slip. This is analogous to material failure by plastic yielding or fracture, where the limiting stress is a function of the principal stresses [35]. The value of L_s^o and e_c are constants associated with a given wall-fluid pair. It must be noted that the asymptotic value L_s^o and e_c is approximately the same as that evaluated for a single phase Couette flow, Fig. 2. Hence, we can say that Thompson & Troian's [22] slip model is the zero-linear-strain-rate limit of this universal relation and in turn, Navier's/Maxwell's [24, 25] model is the low-shear-rate limit of Thompson & Troian's model.

Knowing L_s^o and e_c for a given wall-fluid pair, one can evalute the slip length for any given strain rate using the universal relationship for slip length presented here. Thereby, not having to perform computationally expensive MD simulations. The universal relationship for slip length, along with the generalized velocity boundary condition, provides a unified boundary condition for steady Newtonian fluid flows. The unified boundary condition while being consistent in the limits with the no-slip, Navier/Maxwell and Thompson & Troian boundary conditions, is also able to capture the complete physiscs associated with more complex problem such as the moving contact line and corner flow.

VI. CONCLUSION

To summarize, by extending the Maxwell slip model we obtain a generalized velocity boundary condition which shows that, for a general flow, slip velocity is a function of both the shear rate and the linear strain rate. Knowing this, we find that slip length is a function of principal strain rate. By scaling slip length (L_s) with its asymptotic value (L_s^o), and principal strain rate ($e_{1,2}$) with its critical value (e_c), we obtain a universal relationship for slip length, $L_s = L_s^o(1 - e_{1,2}/e_c)^{-1/2}$. The universal relationship for slip length, together with the generalized velocity boundary condition, gives a unified boundary condition that describes slip at the boundary for a wide range of steady Newtonian flows. This was validated using molecular dynamics simulations for the moving contact line and the corner flow problems. The boundary condition captures the physics associated with complex problems, such as

single-phase corner flows and two-phase moving contact lines, while also being consistent with the slip models of Navier/Maxwell and Thompson & Troian, for simpler flows. Our results suggest that the moving contact line and the corner flow problems, both of which exhibit boundary singularities, are fundamentally similar in nature and are governed by the flow conditions presented here.

ACKNOWLEDGMENT

This research was supported by the Office of Naval Research. We would also like to thank Dr. A. C. DeVoria for his helpful discussion and comments.

(a)

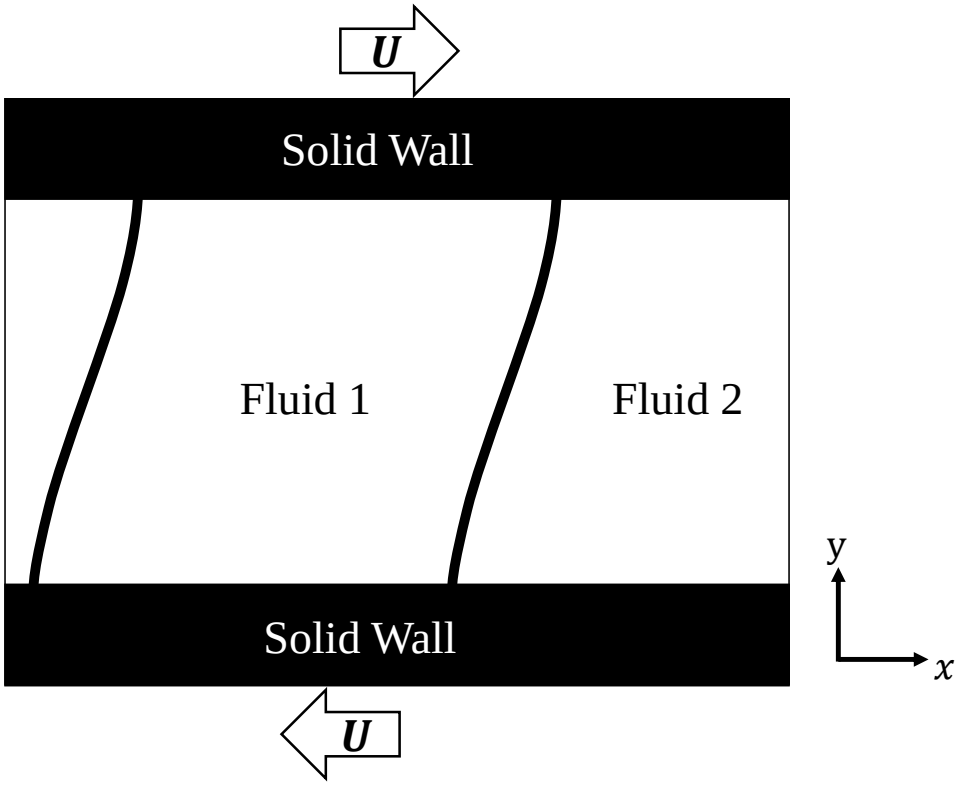

(b)

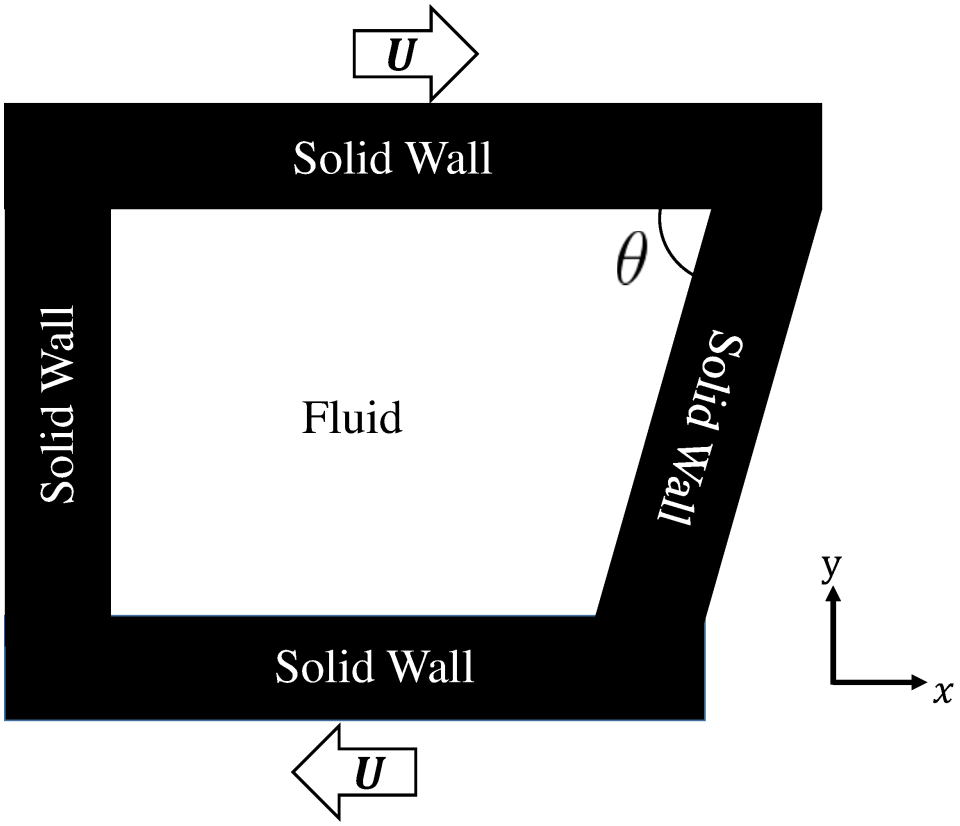

FIG. 1. **Schematics of the problem geometry.** Schematics for, (a) a moving contact line problem and, (b) a corner flow problem.

(a)

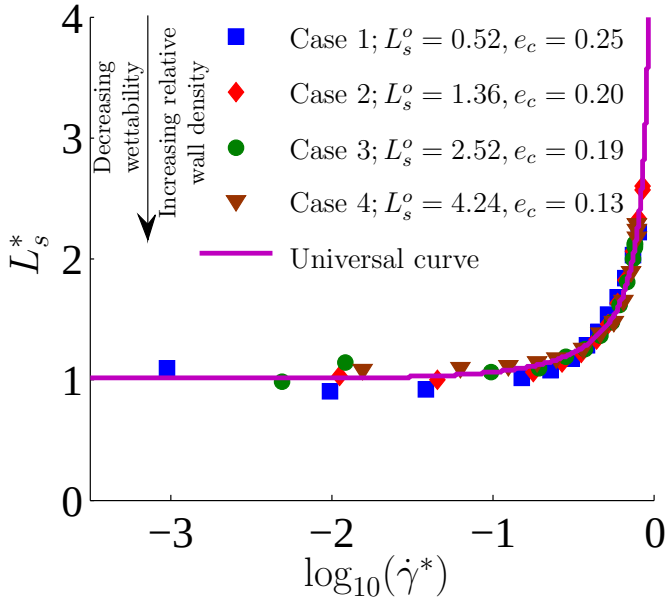

(b)

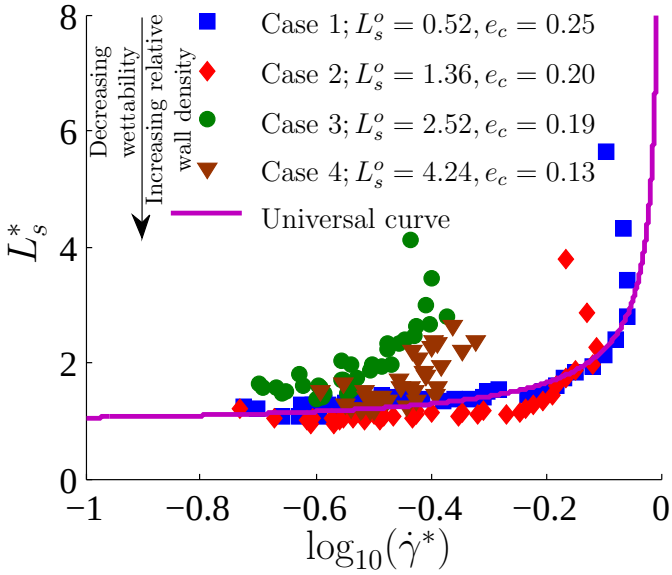

FIG. 2. **Breakdown of Thompson & Troian's slip model for a moving contact line problem.** Scaled slip length versus shear rate is plotted for (a) a single phase unidirectional Couette flow problem and (b) a two-phase, moving contact line problem. For both plots the properties of primary fluid is the same ($\rho \approx 0.73\sigma^{-3}$ and $T = 1.1k_B/\epsilon$). The different cases correspond to different wall-fluid properties, where hydrophobicity increases from Case 1 to 4. As predicted by Thompson & Troian, the data for a single phase Couette flow collapses to a single curve. However, the same scaling does not result in the collapse of data for moving contact line problem. Here, e_c is the critical principal strain rate. The principal strain for a single phase Couette flow is computed as $e_{1,2} = 1/2(\partial u/\partial y + \partial v/\partial x)$. Hence, in the case of a steady incompressible single phase Couette flow the critical principal strain rate is half of the critical shear rate, $e_c = (1/2)\dot{\gamma}_c$.

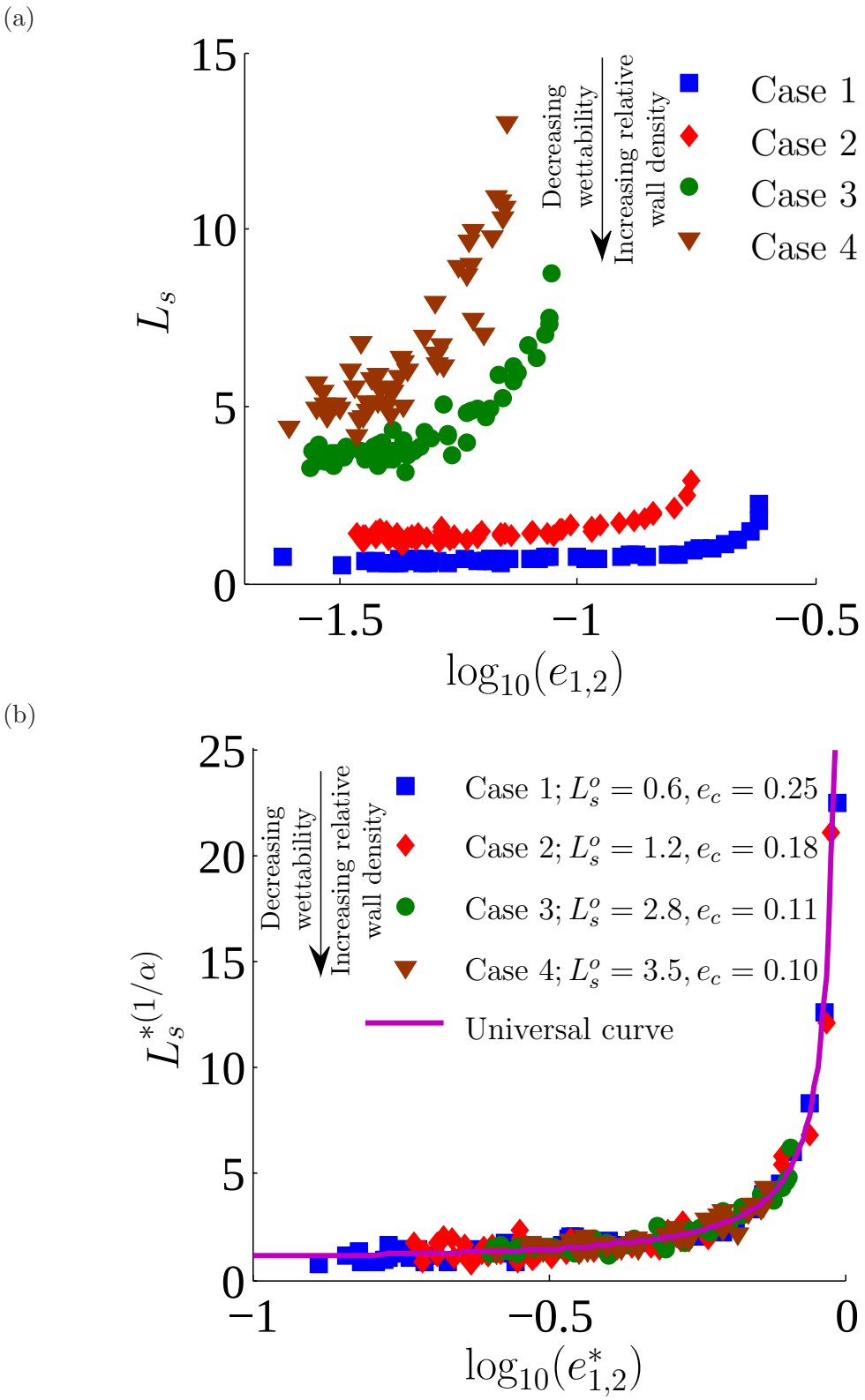

FIG. 3. **Moving contact line: Slip length versus principal strain rate at the trailing edge.** (a) Unscaled data and (b) scaled data. Results are presented for four different cases of wall-fluid properties.

(a)

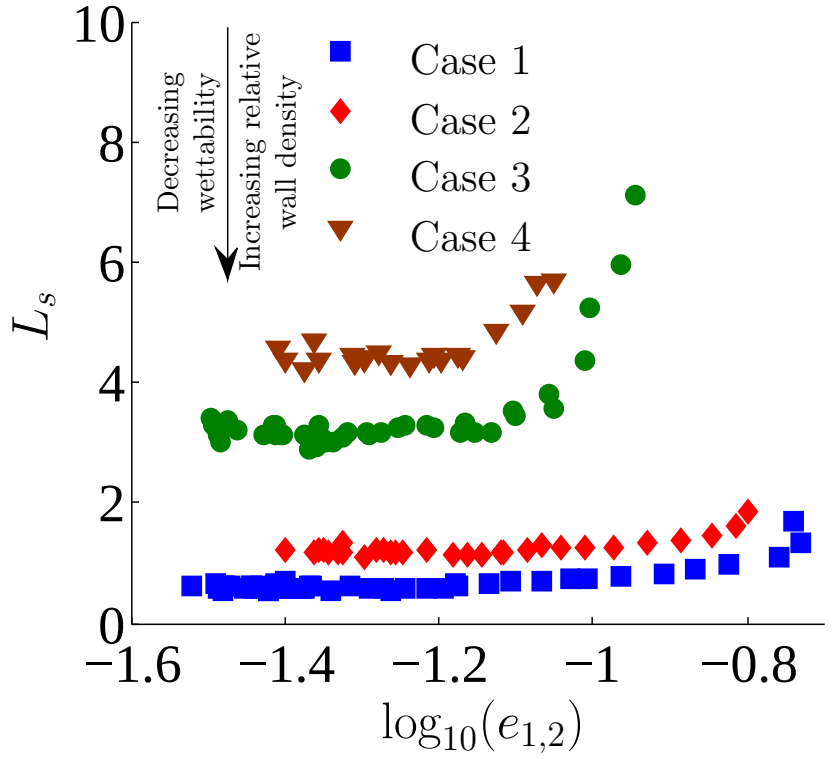

(b)

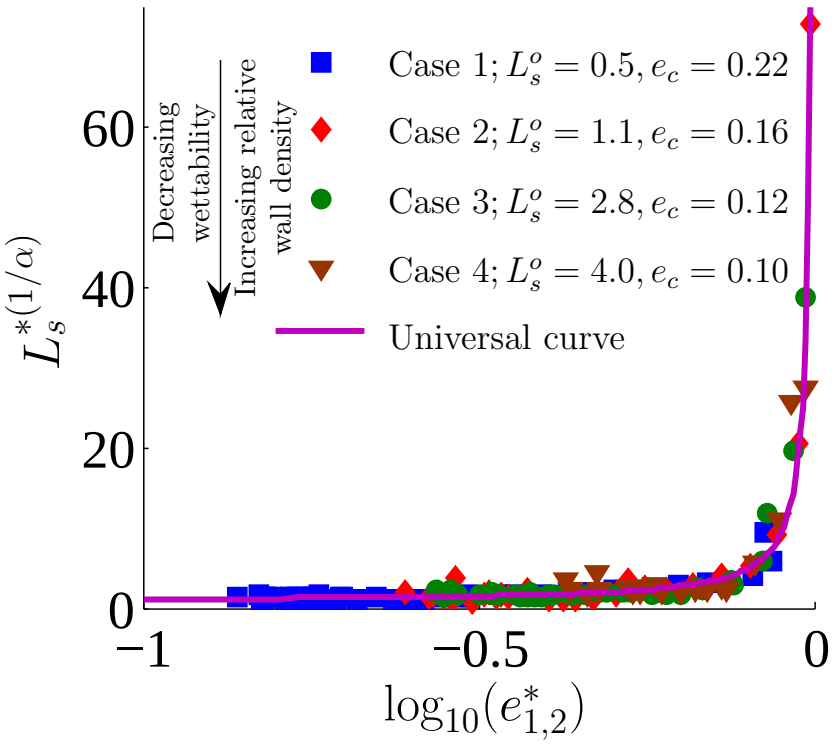

FIG. 4. **Moving contact line: Slip length versus principal strain rate at the leading edge.** (a) Unscaled data and (b) scaled data. Results are presented for four different cases of wall-fluid properties.

(a)

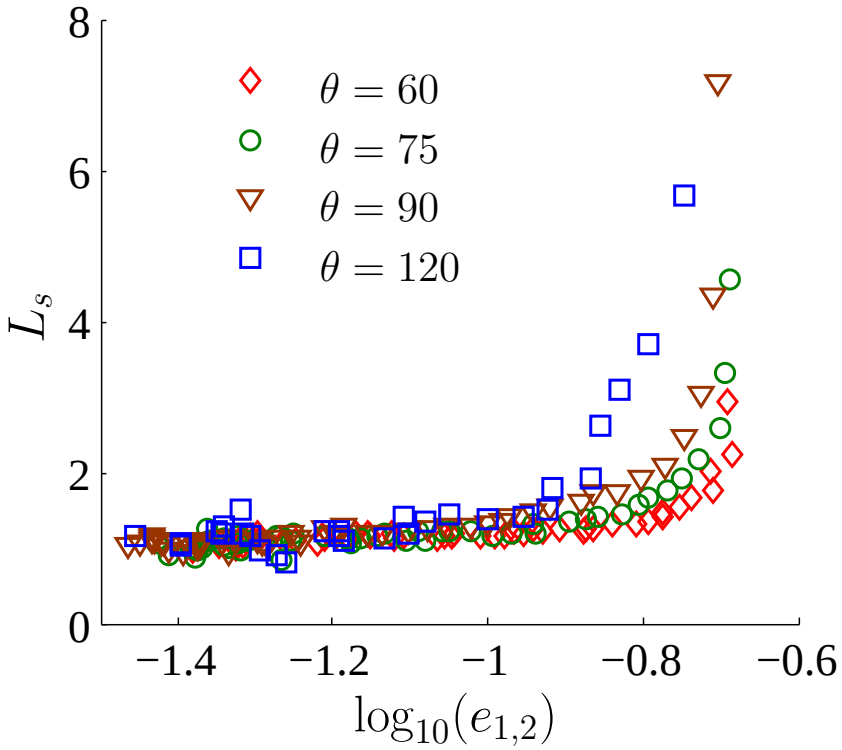

(b)

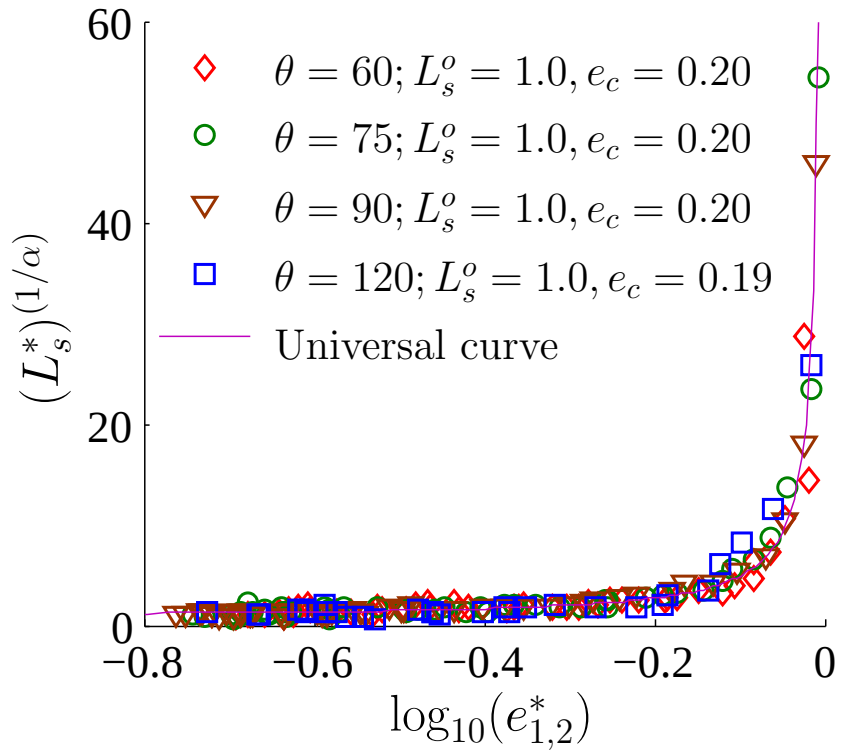

FIG. 5. **Corner flow: Slip length versus principal strain rate at the edge where wall is moving towards the corner.** (a) Unscaled data and (b) scaled data. Results are presented for different contact angles and for wall-fluid properties corresponding to Case 2.

(a)

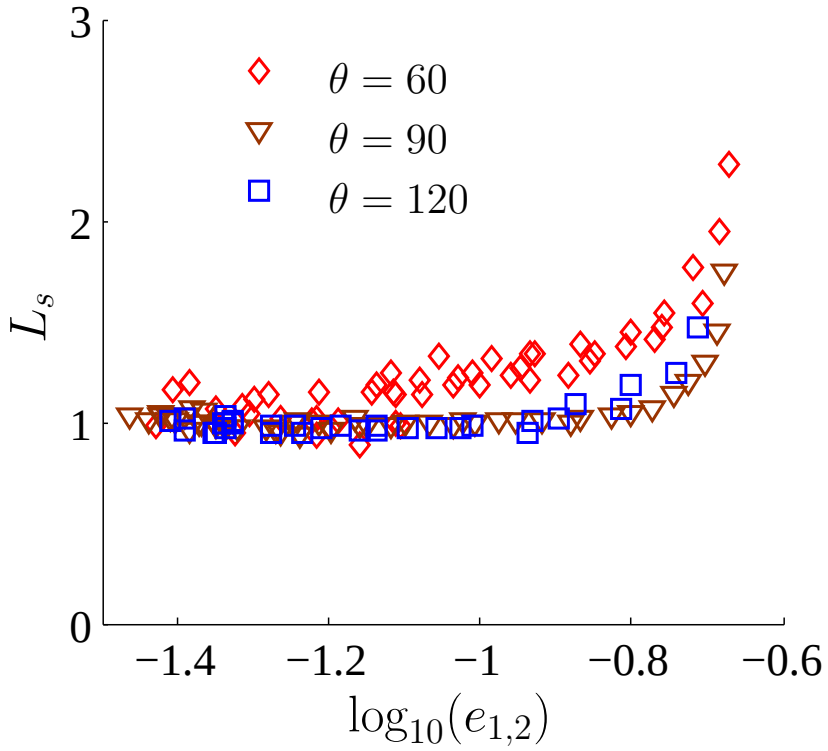

(b)

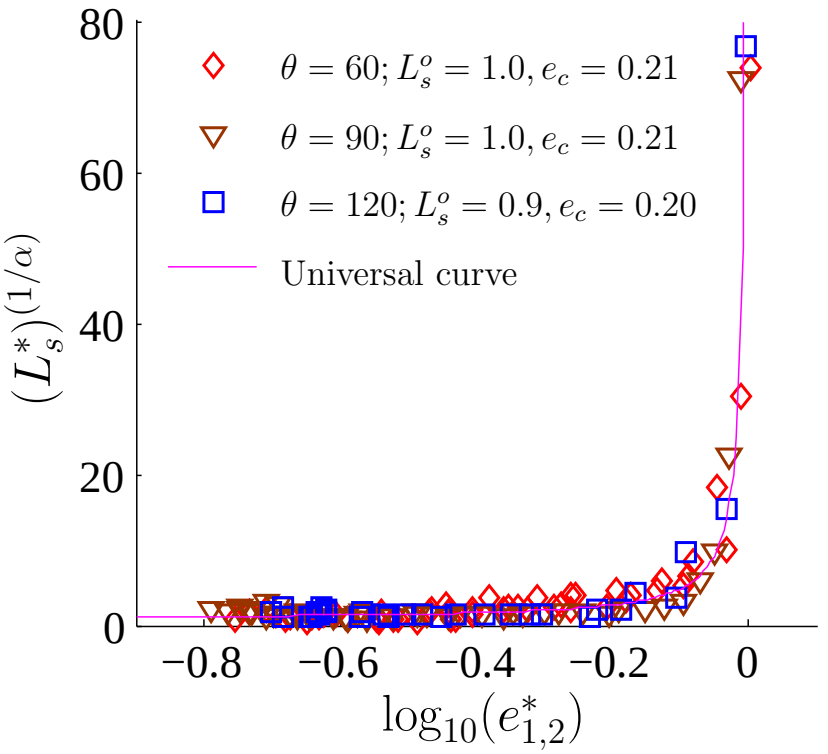

FIG. 6. **Corner flow: Slip length versus principal strain rate at the edge where wall is moving away from the corner.** (a) Unscaled data and (b) scaled data. Results are presented for different contact angles and for wall-fluid properties corresponding to Case 2.

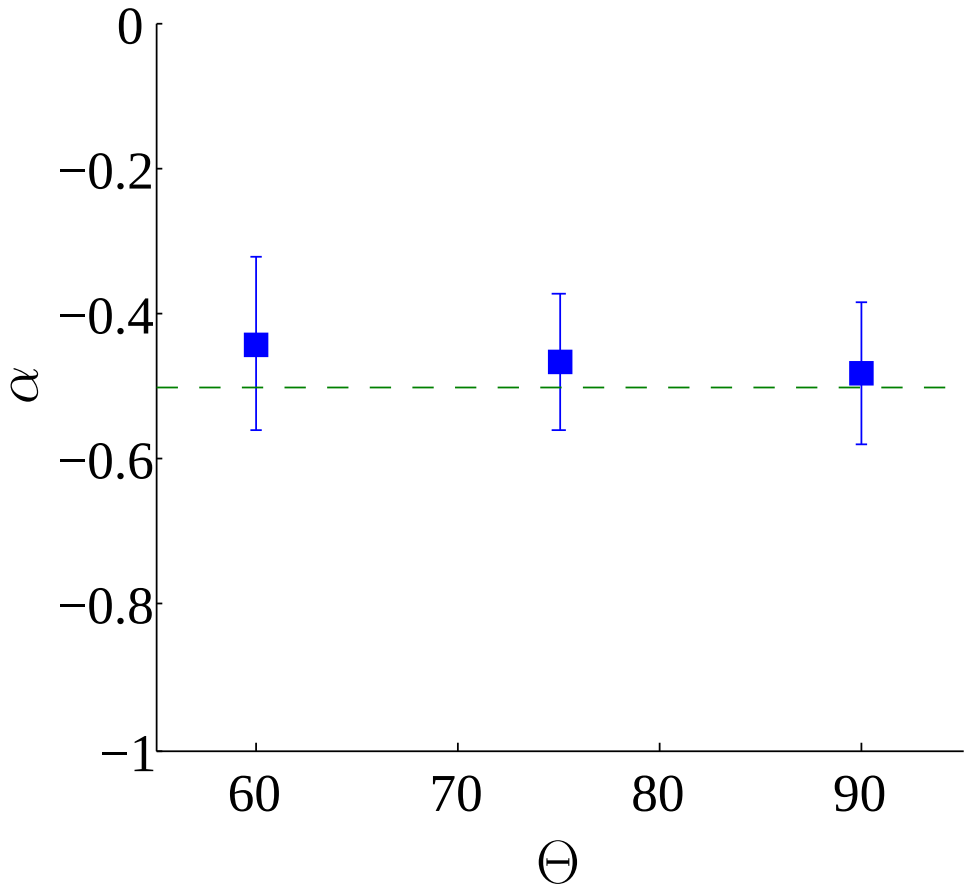

FIG. 7. α **for different corner angles** θ**.** The parameter α is seen to be approximately -0.5, when the results are computed at a reference plane $0.5\sigma^{wf}$ away from the wall lattice site. This is consistent with Thompson & Troian. If the values are not evaluated at the reference plane then α could show corner/contact angle dependency.

[1] S. Goldstein, "Modern development in fluid dynamics," (Clarendon Press Oxford, 1938) pp. 676–680

.

[2] S. Goldstein, Ann. Rev. Fluid Mech. **1**, 1 (1969)

.

[3] O. Vinogradova, Int. J. Miner. Process **56**, 31 (1999)

.

[4] L. Bocquet and J. L. Barrat, Int. J. Miner. Process **3**, 685–693 (2007)

.

[5] B. Y. Cao and M. Sun and Z. Y. Guo, Int. J. Mol. Sci. **10**, 4638–4706 (2009)

.

[6] W. M. Zhang and G. Meng and X. Wei, Microfluid Nanofluid **13**, 845-882 (2012)

.

[7] S. Razavi and J. Koplik and I. Kretzschmar, Langmuir **30**, 11272-11283 (2014)

.

[8] C. Huh and L. Scriven, J. Colloid Interface Sci. **35**, 85 (1971)

.

[9] L. Hocking and A. Rivers, J. Fluid. Mech. **121**, 425 (1982)

.

[10] E. Dussan, Ann. Rev. Fluid Mech. **11**, 37 (1979)

.

[11] P. A. Thompson and M. O. Robbins, Phys. Rev. Lett. **63**, 766 (1989)

.

[12] J. H. Snoeijer and B. Andreotti, Annu. Rev. Fluid Mech **45**, 269–292 (2013)

.

[13] P. G. de Gennes, Rev. Mod. Phys. **57**, 3:827–863 (1985)

.

[14] T. Qian and X. P. Wang and P. Sheng, Comm. Comp. Phys. **1**, 1–52 (2006)

.

[15] H. Moffatt, J. Fluid. Mech. **18**, 1 (1964)

.

[16] J. Koplik and J. Banavar, Physics of Fluids **7**, 3118 (1995)

.

[17] P. N. Shankar and M. D. Deshpande, J. Fluid Mech. **32**, 93–136 (2000)

.

[18] S. Richardson, J. Fluid. Mech. **59**, 707 (1973)

.

[19] S. G. Hatzikiriakos, Int. Poly. Proc. **25**, 55-62 (2010)

.

[20] Z. Ren and X. Huang and H. Liu, Poly. Eng. Sci. **56**, 328–341 (2016)

.

[21] W. Chen and R. Zhang and J. Koplik, Phys. Rev. E **89**, 023005 (2014)

.

[22] P. A. Thompson and S. M. Troian, Nature **389**, 360 (25 September 1997)

.

[23] L. Guo and S. Chen and M. O. Robbins, Phys. Rev. E **93**, 013105 (2016)

.

[24] C.L.M.H. Navier. Memoire sur les lois du mouvement des fluides. *Memoires de l Academie Royale des Sciences de l Instituede France*, 6:389–440, 1823.

[25] J.C. Maxwell. The scientific papers of James Clerk Maxwell. volume V2, pages 703–711, 1890.

[26] S. Plimpton, J. Comp. Physics **117**, 1 (1995)

.

[27] L. Verlet, Phys. Rev. **159** (July 1967)

.

[28] N. V. Priezjev, J. Chem. Phys. **127**, 144708 (2007)

.

[29] A. AlizadehPahlavan and J. B. Freund, Phys. Rev. E **83**, 021602 (2011)

.

[30] L. Loeb, *The Kinetic Theory of Gases* (McGraw-Hill Book Company, 1934)

.

[31] T. Gombosi, *Gaskinetic theory* (Cambridge University Press, 1994)

.

[32] J. J. Thalakkottor and K. Mohseni, Phys. Rev. E **87**, 033018 (2013)

.

[33] P. Chambre and S. Schaaf, *Flow of rarefied gases* (Princeton University Press, 1961)

.

[34] T. Qian and X. P. Wang and P. Sheng, Phys. Rev. E **68**, 016306(15) (2003)

.

[35] A. Nadai, *Theory of Flow and Fracture of Solids* (McGraw-Hill, New york, 1950)

.